EDINBURGH INSTRUMENTS

50 YEARS 1971-2021


# PRECISION RAMAN

**Best-in-class Raman microscopes**
for research and analytical requirements backed with world-class customer support and service.

edinst.com

Research Article

Journal of RAMAN SPECTROSCOPY

Received: 2 August 2010 Accepted: 11 January 2011 Published online in Wiley Online Library: 23 February 2011

(wileyonlinelibrary.com) DOI 10.1002/jrs.2910

# Synthesis and Raman spectroscopic investigation of a new self-assembly monolayer material 4-[*N*-phenyl-*N*-(3-methylphenyl)-amino]-benzoic acid for organic light-emitting devices

**M. Kurt,[a]* S. Okur,[b] S. Demic,[c] J. Karpagam[d] and N. Sundaraganesan[d]**

**We have synthesized 4-[*N*-phenyl-*N*-(3-methylphenyl)-amino]-benzoic acid (4-[PBA]) and investigated its molecular vibrations by infrared and Raman spectroscopies as well as by calculations based on the density functional theory (DFT) approach. The Fourier transform (FT) Raman, dispersive Raman and FT-IR spectra of 4-[PBA] were recorded in the solid phase. We analyzed the optimized geometric structure and energies of 4-[PBA] in the ground state. Stability of the molecule arising from hyperconjugative interactions and charge delocalization was studied using natural bond orbital analysis. The results show that change in electron density in the $\sigma^*$ and $\pi^*$ antibonding orbitals and $E_2$ energies confirm the occurrence of intramolecular charge transfer within the molecule. Theoretical calculations were performed at the DFT level using the Gaussian 09 program. Selected experimental bands were assigned and characterized on the basis of the scaled theoretical wavenumbers by their total energy distribution. The good agreement between the experimental and theoretical spectra allowed positive assignment of the observed vibrational absorption bands. Finally, the calculation results were applied to simulate the Raman and IR spectra of the title compound, which show agreement with the observed spectra.** 

*Supporting information may be found in the online version of this article.*

**Keywords:** FT-Raman; dispersive Raman; DFT; NBO; 4-[*N*-phenyl-*N*-(3-methylphenyl) amino]-benzoic acid

## Introduction

Triphenylamine and several of its derivatives have drawn the attention of photoscientists because of their huge potential in diverse fields. These compounds have found application in organic light-emitting diodes (OLEDs) particularly in the blue region,[1–9] as photoconductors[10] as well as semiconductors.[7–9] Since the initial work by Tang and Van Slyke,[11] the thin, multilayer OLEDs have been recognized as one of the potential technologies for next-generation flat-panel display devices.[11,12] The simplest multilayer OLED consists of indium tin oxide as anode, an electron-transporting material (ETM) layer, a hole-transporting material (HTM) layer and a cathode, in which HTM or/and ETM can act as light emitters.[11] The HTM must have a lower energy barrier to inject holes from the anode, a higher mobility and thermally stability in the amorphous state.[13–19] Although the guidelines for designing the HTM with these requirements are well known, the guidelines on the mobility of charge carriers in HTM are limited since experimental data in this area are scarce.[20] While there is much interest in the chemical synthesis of the organic hole-transporting devices, an important research frontier area is the fundamental mechanism of charge transport in these materials.[18–22]

The IR, Fourier transform (FT) Raman and dispersive Raman spectroscopy combined with quantum chemical computations have been recently used as an effective tool in the vibrational analysis of drug molecules,[23] biological compounds[24] and natural products,[25] since fluorescence-free Raman spectra and the computed results can help unambiguous identification of the vibrational modes as well as the bonding and structural features of complex organic molecular systems. Both IR and Raman spectroscopy analysis have been used to elucidate the structural information on molecules.

In this work, we synthesized and report the experimental and theoretical Raman studies of 4-[PBA] in an effort to obtain a deeper insight into the molecule. In the following, we discuss the mid-IR, FT-Raman and dispersive Raman spectrum of 4-[PBA] at room temperature (rt), assigning vibrational wavenumbers using density functional theory (DFT) calculations.

* *Correspondence to: M. Kurt, Department of Physics, Ahi Evran University, Kırşehir 40100, Turkey. E-mail: kurt@gazi.edu.tr*

a *Department of Physics, Ahi Evran University, Kırşehir 40100, Turkey*

b *Department of Physics, Faculty of Science, Izmir Institute of Technology, Izmir, Turkey*

c *Solar Energy Institute, Ege University, Izmir 35040, Turkey*

d *Department of Physics (Engg.), Annamalai University, Annamalai Nagar, Tamil Nadu 608002, India*

Journal of RAMAN SPECTROSCOPY

## Experimental

### Synthesis

The title compound was synthesized using the following procedures:

Ethyl 4-[(3-methylphenyl)(phenyl)amino]benzoate (**1**)[26]: To a mixture of *N*-(3-methylphenyl)-*N*-phenylamine (1.1 g, 6.4 mmol) and ethyl 4-bromobenzoate (1.3 g, 6.0 mmol) in dry toluene (18 ml) was added *t*-BuONa (0.75 g, 7.0 mmol), P(*t*-Bu)$_3$ (0.12 g, 0.5 mmol) and palladium acetate (0.06 g, 0.25 mmol) in the given sequence. The resulting mixture was heated to 120 °C for 28 h. After cooling to rt, the reaction mixture was quenched by distilled water (40 ml) and extracted by ethyl acetate (40 ml). The organic phase was washed successively with distilled water and brine, and then dried over anhydrous magnesium sulfate. The crude product was chromatographed (silica gel, dichloromethane : *n*-hexane, 1 : 1) to give a light brown oil (1.21 g, 60%).

Sodium 4-[(3-methylphenyl)(phenyl)amino]benzoate (**2**)[27] and 4-[(3-methylphenyl)(phenyl)amino]benzoic acid (4-[PBA]): An aqueous solution of NaOH (5 equiv., 2 N) was added to **1** (1 equiv.), which was dissolved previously in methanol/THF (30 ml, 1 : 1), at 0 °C. After stirring for 12 h at rt, the reaction mixture was subjected to vacuum and the residue dissolved in water. After washing with ethyl acetate, the aqueous phase was acidified with formic acid (50% in water, 5 equiv.) and subsequently extracted with EtOAc (3 × 25 ml). The combined organic layers were dried over sodium sulfate. Removal of the solvent provided the title compound 4-[PBA] with 70% yield, which was then used without further purification.

$^1$H NMR (400 MHz, $CDCl_3$, TMS): 7.91 (d, 2H), 7.31 (t, 2H), 7.21 (t, 2H), 7.16–7.11 (m, 2H), 6.98 (m, 6H), 2.29 (s, 3H).

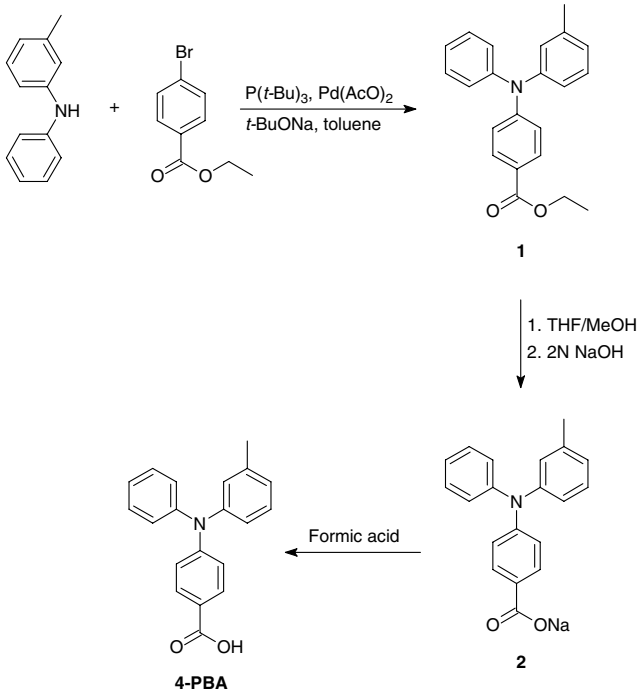


The title compound 4-[PBA] was synthesized after three steps in the powder form following published protocols and it was used as such without further purification. The FT-Raman spectrum of 4-[PBA] was recorded using the 1064 nm line of an Nd : YAG laser as excitation wavelength in the region 3500–100 cm$^{-1}$ on a Bruker optics IFS 66 model spectrometer with the spectral resolution of 4 cm$^{-1}$, as shown in Fig. 1. The Raman spectra of the complexes were recorded in the range 4000–250 cm$^{-1}$ on a Bruker Senterra dispersive Raman instrument using 532, 633, and 785 nm laser excitation, but 532 and 633 nm excitations did not provide any spectra. The FT-IR spectrum was recorded on KBr pellets as shown in Fig. S2 (Supporting information). The pellets were prepared by mixing together 1 mg of the sample with 99 mg of KBr and pressed to make a thin transparent film. The FT-IR spectrum of the sample was recorded in the transmission mode using a Mattson 1000 FT-IR spectrometer in the range 4000–400 cm$^{-1}$ with a spectral resolution of 4 cm$^{-1}$.

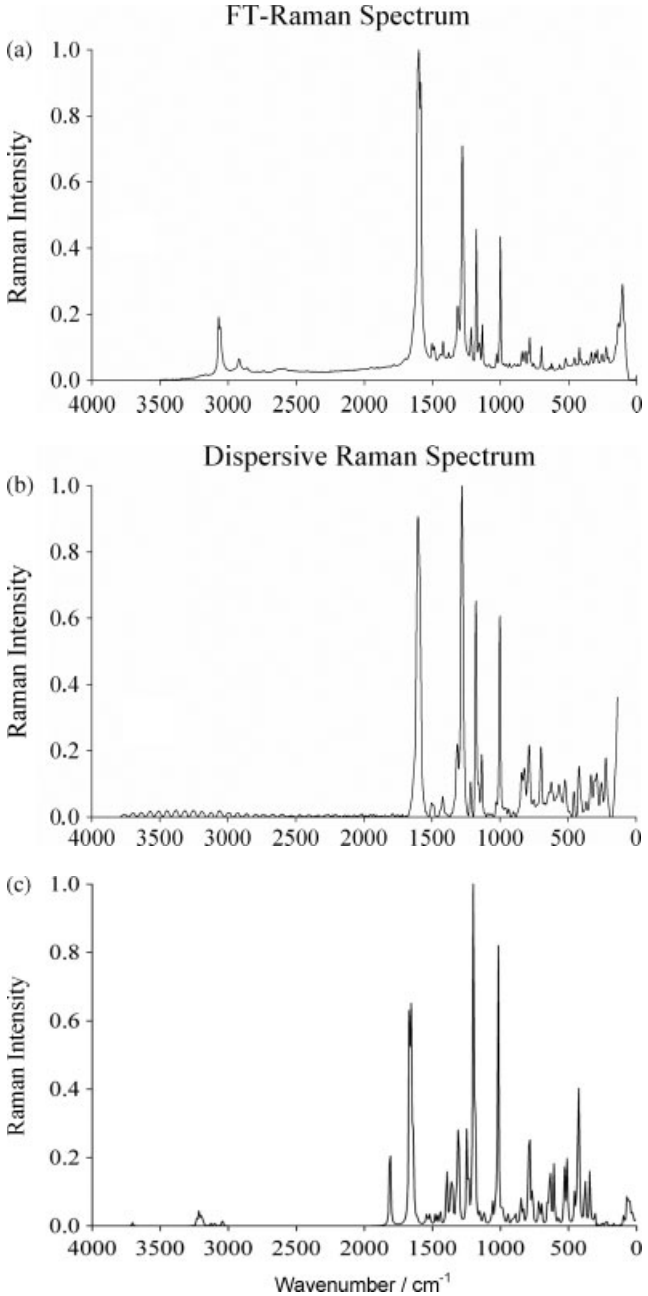


**Figure 1.** (a) FT-Raman spectrum of 4-[PBA], (b) dispersive Raman spectrum of 4-[PBA], and (c) simulated Raman spectrum of 4-[PBA].



  

## Computational Details and Raman Intensity

The entire set of calculations was performed at the DFT level on a personal computer using the Gaussian 09[28] program package, invoking gradient geometry optimization.[29] The Raman activities ($S_{Ra}$) calculated with the same program[28] were converted to relative Raman intensities ($I_{Ra}$) using the following relationship derived from the intensity theory of Raman scattering[30,31]:

$$I_i = \frac{f(\nu_0 - \nu_i)^4 S_i}{\nu_i[1 - \exp(-hc\nu_i/kT)]} \quad (1)$$

where $\nu_0$ is the wavenumber of the exciting laser (in this work, we have used the excitation wavenumber $\nu_0 = 9398.5\ cm^{-1}$, which corresponds to the wavelength of 1064 nm of the Nd : YAG laser), $\nu_i$ is the vibrational wavenumber of the *i*th normal mode (in $cm^{-1}$) and $S_i$ is the Raman scattering activity of the normal mode $\nu_i$. $f$ (a constant equal to $10^{-12}$) is a suitably chosen common normalization factor for all peak intensities. $h$, $k$, $c$ and $T$ are the Planck and Boltzmann constants, the speed of light and the temperature in kelvin, respectively.

The optimized structural parameters were used in the vibrational wavenumber calculations at the DFT level to characterize all stationary points as minima. In the present work, we have used the DFT/B3LYP approach with 6-311++G(d) and 6-311++G(d,p) as basis sets for the computation of molecular structure and energies of the optimized structures. The optimized structural parameters were used in the vibrational wavenumber calculation at the DFT level to characterize all stationary points as minima. The vibrational wavenumber calculations were carried out using the standard basis set 6-31G(d). The total energy distribution (TED) was calculated by using the scaled quantum mechanics (SQM) program,[32,33] and the fundamental vibrational modes were characterized by their TED.

The natural bonding orbital (NBO) calculations[34] were performed using the NBO 3.1 program as implemented in the Gaussian 03 W[28] package at the DFT/B3LYP/6-311G(d,p) level in order to understand various second-order interactions between the filled orbitals of one subsystem and vacant orbitals of another subsystem, which is a measure of the intermolecular delocalization or hyper conjugation.

## Results and Discussion

### Molecular geometry

The optimized structure parameters of 4-[PBA] calculated at the DFT(B3LYP) level with 6-311++G(d) and 6-311++G(d,p) basis sets are listed in Table S1 (Supporting information) in accordance with atom numbering scheme given in Fig. S1. Table S1 (Supporting information) compares the calculated bond lengths and angles for 4-[PBA] with those experimentally available from X-ray data of a closely related molecule such as triphenylamine.[35] From the DFT theoretical values, we find that most of the optimized bond lengths are overestimated or underestimated when compared with experimental values; this is due to the fact that the theoretical calculations were based on an isolated molecule in the gaseous phase but the experimental results are based on the molecule in the solid state.

The interaction of both the COOH and $CH_3$ groups on the benzene ring of 4-[PBA] is of great importance in determining its structure and vibrational properties. In this structure, the central nitrogen and the three adjacent carbon atoms are coplanar as is evident from the torsional angles N1–C12–C13–C15 = −179.07°, N1–C2–C4–C7 = −179.66° and N1–C22–C24–C27 = 179.62°. The same behavior was also reported for triphenylamine.[36]

The COOH and $CH_3$ groups are coplanar with respect to the benzene ring as is evident from torsional angles C15–C19–C17–C33 = −179.26° and C3–C5–C9–C37 = −179.84°. The average C–C bond length of 1.399 ´Å agrees very well with that of a standard molecule (benzene). Comparison of the experimental and calculated NCC bond angles showed that the C2–N1–C12 and C2–N1–C22 angles are larger by 2° when compared with the C12–N1–C22 bond angle. On the other hand, the appearance of substituents on the benzene ring can cause a difference among the C–C distances. The C–C bond lengths of the benzene rings appear little distorted with C12–C13, C12–C14, C2–C4, C2–C3, C22–C23, and C22–C24 bond distances (~1.40 ´Å) slightly longer than the rest of the substituents (1.39 ´Å). The N1–C12 (1.428 ´Å) and N1–C22 (1.426 ´Å) distances are longer than the N1–C2 distance (1.405 ´Å).

### Vibrational spectral analysis

The molecular structure of 4-[PBA] in the ground state was optimized by the B3LYP method with the 6-311++G(d,p) and 6-311++G(d) basis sets. The vibrational wavenumbers were calculated with using the 6-31G(d) basis set and then scaled by 0.9614.[37] The molecule consists of 40 atoms. It has 114 normal vibrational modes. All the vibrations are active both in the infrared and Raman spectrum. The simulated vibrational Raman and IR spectra are given in Fig. 1 and Fig. S2. The TED of the vibrational modes was calculated using the SQM program.[32,33] In Table 1, we have presented the calculated vibrational wavenumbers, IR intensities and Raman scattering activities along with measured experimental vibrational wavenumbers. In spite of the good agreement between the experimental and calculated spectra, as usual the theoretical wavenumbers are slightly overestimated, mainly due to the neglecting of anharmonicity.

#### *C–H vibrations*

The hetero aromatic structure shows the presence of C–H stretching vibration in the region 3100–3000 $cm^{-1}$, which is the characteristic region for the ready identification of C–H stretching vibration.[38] In this region, the bands are not affected appreciably by the nature of the substituent. The 4-[PBA] molecule has 13 C–H moieties in the aromatic ring systems as shown in Fig. S1. The expected 13 C–H stretching vibrations correspond to the stretching modes of C3–H, C5–H, C4–H, C7–H, C13–H, C14–H, C15–H, C19–H, C23–H, C24–H, C25–H, C27–H and C29–H units. Hence, in our present work the band observed at 3068 $cm^{-1}$ in FT-Raman spectrum is assigned to C–H stretching vibration. The scaled vibration (mode no: 113–101) by the B3LYP/6-31G(d) method predicted at 3103–3054 $cm^{-1}$ falls within the recorded spectral data. The in-plane aromatic C–H bending vibration occurs in the region 1300–1000 $cm^{-1}$; the bands are sharp but they are of weak to medium intensity. The C–H in-plane bending vibration computed (mode nos: 75-57) by the B3LYP/6-31G(d) method at 1271–976 $cm^{-1}$ shows good agreement with the measured FT-IR bands at 1281, 1175, 1129, 1082 and 1028 $cm^{-1}$ and with the measured FT-Raman bands at 1280, 1177, 1155, 1133 and 1001 $cm^{-1}$. The theoretically computed C–H out-of-plane bending vibrations for 4-[PBA] also show good agreement with the recorded spectrum as shown in Table 1.

**Table 1.** Calculated vibrational wavenumber, measured IR and Raman band positions ($cm^{-1}$) and assignments for 4-[PBA]

| Mode no. | Experimental wavenumber ($cm^{-1}$) FT-IR | FT-Raman | Dispersive Raman | Theoretical wavenumber ($cm^{-1}$) Scaled | $IR_{int}$ | $S_{act}$ | $R_{Int}$ | TED (≥10%) |
|---|---|---|---|---|---|---|---|---|
| 1 | | | | 25 | 0.83 | 0.71 | 76.87 | Tors. CC NC (73) |
| 2 | | | | 30 | 2.14 | 1.23 | 89.42 | Tors. CCNC (56) |
| 3 | | | | 37 | 0.58 | 1.22 | 64.00 | Tors. CCCN(11) + tors. CC NC(60) |
| 4 | | | | 47 | 0.49 | 2.61 | 84.99 | Tors. CC NC (6) + tors. HCCC(68) |
| 5 | | | | 49 | 0.37 | 4.29 | 129.69 | Bend CNC(11) + tors. CC NC(22) + HCCC(24) |
| 6 | | | | 58 | 0.38 | 9.16 | 205.22 | Tors. CCNC (45) + tors. OCCC(34) |
| 7 | | | | 67 | 0.01 | 13.61 | 230.64 | Bend CNC (28) + tors. CCNC(38) |
| 8 | | | | 90 | 0.95 | 6.69 | 67.06 | Tors. CCNC (38) + tors. OC CC (47) |
| 9 | | 106m | | 115 | 0.36 | 0.57 | 3.75 | Bend CNC (12) + tors. CCNC, CCCC (21) + tors. CCCH (10) |
| 10 | | 134w | | 162 | 1.36 | 2.50 | 9.35 | Bend CCN, CCC (55)+ bend OCC (15) |
| 11 | | | | 207 | 2.64 | 4.38 | 11.17 | tors CCC C (55) + tors. H CC C (10) |
| 12 | | | | 217 | 0.42 | 6.12 | 14.58 | Bend CCN, CCC (18) |
| 13 | | 224w | 222w | 224 | 1.12 | 1.18 | 2.68 | Bend CCN, CCC, OCC (20) + tors. CCCN, CCCC(15) |
| 14 | | | | 240 | 2.02 | 4.46 | 9.13 | Bend CCN (24) + tors. CCC N, CCCC(11) |
| 15 | | | 254w | 251 | 0.81 | 2.74 | 5.23 | Bend CCN, CC(30) + tors.CCCN, CCCC(15) |
| 16 | | 290w | 288w | 277 | 1.24 | 3.64 | 6.04 | Bend CNC, CCN, CCN(17) + tors. CCCN, OCC C(37) |
| 17 | | 333w | 330w | 329 | 0.34 | 2.09 | 2.72 | Bend C N, C NC, CC C, OCC (49) |
| 18 | | | 365w | 364 | 3.06 | 3.00 | 3.39 | Bend CCN, CCC (57) |
| 19 | | | | 404 | 3.66 | 2.89 | 2.83 | Bend CCCC, CCCN (53) + tors. CCCH (23) |
| 20 | | | | 409 | 4.50 | 7.35 | 7.10 | Tors. CC CC, CCCN (59) + tor.s CCCH, HCCC (15) |
| 21 | | 421w | 418w | 417 | 6.07 | 4.19 | 3.94 | Str. CC (11) + bend CCC, CCN, OCC, OCO (30) |
| 22 | | | | 435 | 6.24 | 1.37 | 1.22 | Bend CCN, C C C, OCO(23) + tors. CCCC (15) |
| 23 | 451w | | 456w | 439 | 5.36 | 1.48 | 1.22 | Bend CCN, CCC (23)+ tors. C C C N, CCCC (19) |
| 24 | | | | 487 | 22.82 | 1.75 | 1.34 | Bend CCC, OCC (33) |
| 25 | | | | 491 | 10.07 | 5.33 | 4.03 | Bend CCN, CCC, OCC(31) |
| 26 | 500w | | | 506 | 14.42 | 4.56 | 3.31 | Str. C (16) + bend CCC (26) |
| 27 | 518w | | 521w | 511 | 14.85 | 2.61 | 1.88 | Bend CCC(14) + tors. CCCC, CCC H(16) |
| 28 | 546w | | | 550 | 18.73 | 1.15 | 0.74 | Tors. CC NC, H CCC, CCCN, CCCC (30) |
| 29 | 565w | | | 582 | 52.11 | 9.80 | 5.91 | Tors. HOCC, HOCO (73) |
| 30 | | | | 606 | 0.95 | 6.66 | 3.79 | Bend CCC, HCC(69) |
| 31 | | | | 613 | 5.91 | 4.85 | 2.72 | Bend CCC, CNC (27) |
| 32 | | | | 618 | 18.30 | 0.50 | 0.27 | Bend CCC, OCC, OCO, HOC (45) |
| 33 | 638w | | | 626 | 5.81 | 5.50 | 2.99 | Bend CCC, CCC (36) |
| 34 | | | | 670 | 11.00 | 4.69 | 2.33 | Bend CCC, OCO(21) |
| 35 | | | | 681 | 20.63 | 0.54 | 0.24 | Tors. CCCC, C CCH, HCCC (69) |
| 36 | | | | 687 | 35.74 | 3.65 | 1.75 | Tors. CCCC, CCCH, HOCO (9) |
| 37 | 696s | 699mw | | 690 | 54.22 | 3.29 | 1.57 | Tors. CCCC, CCCH, HOCO, OCCC(39) |
| 38 | | | | 734 | 25.12 | 10.73 | 4.71 | Tors. HCCN, HCCC, CCCH(45) |
| 39 | | | | 745 | 50.03 | 0.99 | 0.43 | Tors. HCCC, OCCC, HOCO(61) |
| 40 | 752m | | | 756 | 18.18 | 42.72 | 18.04 | Str. CC, CO(27) |
| 41 | 770m | | | 769 | 11.26 | 5.32 | 2.19 | Tors. H CCN, HCCC, CCCH, HCCH (73) |
| 42 | 798w | 786w | 785mw | 800 | 4.89 | 4.48 | 1.74 | Str. CC, CN(39) |
| 43 | | | | 811 | 0.49 | 4.35 | 1.66 | Tors. H CCN, HCCC, CCCH, HCCH(75) |
| 44 | | 821w | | 817 | 0.23 | 9.73 | 3.68 | Tors. HCCN, HCCC, CCCH, HCCH (77) |
| 45 | 826w | | 830w | 833 | 13.83 | 0.43 | 0.16 | Tors. HCCN, HCCC, CCCH, HCCH (64) |
| 46 | 853w | | 840w | 855 | 1.22 | 6.19 | 2.19 | Tors. HCCN, HCCC, CCCH, HCC H (76) |
| 47 | 873w | | | 871 | 1.19 | 3.43 | 1.18 | Tors. HCCN, HCCC, CCCH, HCC H (62) |
| 48 | | | | 883 | 2.80 | 1.47 | 0.50 | Tors. HCCN, HCCC, CCCH, HCCH (64) |
| 49 | 900w | | 901w | 908 | 0.15 | 6.27 | 2.06 | Str. CC (21) |

**Table 1.** (*Continued*)

| Mode no. | Experimental wavenumber ($cm^{-1}$) FT-IR | FT-Raman | Dispersive Raman | Theoretical wavenumber ($cm^{-1}$) Scaled | $IR_{int}$ | $S_{act}$ | $R_{Int}$ | TED (≥10%) |
|---|---|---|---|---|---|---|---|---|
| 50 | | | | 928 | 0.58 | 0.44 | 0.14 | Tors. HCCN, HCCC, CCCH, HCCH (82) |
| 51 | | | | 935 | 0.14 | 1.27 | 0.40 | Tors. HCCN, HCCC, CCCH (88) |
| 52 | | | | 937 | 1.15 | 1.15 | 0.35 | Tors. HCCN, HCCC, HCCH (81) |
| 53 | 943w | | | 946 | 2.13 | 5.48 | 1.68 | Str. CC, CN (32) + bend CCC, HCC (18) |
| 54 | | | | 950 | 0.51 | 1.79 | 0.54 | Tors. HCCN, HCCC, HCCH (71) |
| 55 | | | | 951 | 0.62 | 2.17 | 0.66 | Tors. H CCH, HCCC(64) |
| 56 | | | | 976 | 0.17 | 103.09 | 30.19 | Str. CC (36) + bend CCC (35) |
| 57 | | | | 976 | 0.04 | 53.44 | 15.63 | Str. CC (30) + bend CCC (39) |
| 58 | | | | 989 | 2.60 | 7.00 | 2.00 | Str. CC (29) + bend HCC, CCC (60) |
| 59 | | | | 997 | 4.62 | 7.23 | 2.05 | Str. C C, CN (16) + bend HCC, CCH (39) |
| 60 | | 1001s | 1000s | 1016 | 5.20 | 16.90 | 4.65 | Str. CC (50) + bend HCC, CCH (21) |
| 61 | 1028w | | | 1032 | 6.75 | 2.20 | 0.60 | Bend HCC, CCH (63) + tors. CCCH (25) |
| 62 | | | | 1069 | 6.59 | 0.59 | 0.15 | Str. CC (42) + bend HCC, CCH (39) |
| 63 | | | | 1073 | 181.43 | 8.25 | 2.10 | Str. OC (48) +str. C C (23) |
| 64 | 1082w | | | 1081 | 1.08 | 4.14 | 1.04 | Str. CC (39) + bend HCC, CCH (39) |
| 65 | | | | 1107 | 3.28 | 8.17 | 1.20 | Str. CC (25) + bend HCC, CCH (56) |
| 66 | 1129w | 1133w | 1133w | 1138 | 6.70 | 83.20 | 19.22 | Str. CC, NC (31) + bend HCC, CCH (24) |
| 67 | | | | 1144 | 2.47 | 5.90 | 1.35 | Str. C C (14) + bend H CC, CCH (75) |
| 68 | | | | 1151 | 443.22 | 294.11 | 66.78 | Str. C C, OC (21) + bend HCC, CCH (40) + HOC (20) |
| 69 | | 1155w | | 1155 | 2.38 | 5.22 | 1.17 | Str. C C (15) + bend HCC, CCH (73) |
| 70 | | | | 1162 | 3.73 | 16.60 | 3.72 | Str. CC (14) + bend HCC, CCH (73) |
| 71 | 1175s | 1177w | 1177s | 1184 | 91.94 | 36.75 | 7.97 | Str. CC(23) + bend HCC, CCH, HOC (58) |
| 72 | | 1216w | 1215w | 1196 | 22.00 | 97.09 | 20.73 | Str. CN, CC (49) |
| 73 | | | | 1256 | 108.37 | 170.87 | 33.71 | Str. CC, NC (57) |
| 74 | | | | 1265 | 46.67 | 13.31 | 2.59 | Str. CN, CC(40) + bend HCC, CCH(19) |
| 75 | 1281m | 1280s | 1279vs | 1271 | 151.20 | 40.69 | 7.86 | Str. CN, CC(46) + bend HCC, CCH(14) |
| 76 | | | | 1296 | 25.39 | 7.93 | 1.48 | Str. CC, CN (12) + bend HCC, CCH (68) |
| 77 | | | | 1301 | 153.07 | 60.06 | 11.17 | Str. CN, CC (45) |
| 78 | | | | 1307 | 7.19 | 12.32 | 2.28 | Str. CC(42) +bend HCC, CCH (38) |
| 79 | | | | 1311 | 4.97 | 27.77 | 5.10 | Str. CC (68) |
| 80 | 1314w | 1314w | 1312m | 1316 | 79.15 | 13.50 | 2.44 | Str. CN(10) + bend HCC, CCH(57) |
| 81 | | | | 1339 | 224.34 | 103.63 | 18.35 | Str. CC, OC(40) + bend OCC, OCO, HOC (43) |
| 82 | | | | 1385 | 0.48 | 30.36 | 5.07 | Bend HCC, HCH (95) |
| 83 | | | | 1406 | 18.58 | 13.88 | 2.26 | Str. CC (37) + bend HCC, CCH (25) |
| 84 | 1423m | 1421w | 1420w | 1421 | 11.28 | 17.94 | 2.87 | Str. CC(29) + bend HCC, CCH (19) |
| 85 | | | | 1441 | 0.84 | 3.05 | 0.48 | Str. CC ((30) + bend HCC, HCH, CCH (48) |
| 86 | | | | 1457 | 4.60 | 16.81 | 2.57 | Bend CCH, HCC, HCH (67)+ tors. HCCC, CCH (27) |
| 87 | | | | 1464 | 5.04 | 8.76 | 1.32 | Bend CCH, HCC, HHC (52) + tors. CCCH, HCCC(19) |
| 88 | | | | 1478 | 97.63 | 12.06 | 1.80 | Str. CC(17) + bend HCC, CC H (39) |
| 89 | 1488m | | | 1481 | 90.83 | 12.74 | 1.89 | Str. CC(25) + bend HCC, CCH(47) |
| 90 | 1509w | 1502w | 1501w | 1494 | 73.65 | 5.03 | 0.73 | Str. CN, CC(36) + bend HCC, CCH (50) |
| 91 | | | | 1547 | 17.18 | 13.71 | 1.88 | Str. CC (68) |
| 92 | | | | 1572 | 10.13 | 18.25 | 2.43 | Str. CC (60) |
| 93 | | | | 1574 | 98.66 | 130.10 | 17.33 | Str. CC (64) |
| 94 | 1584vs | | | 1586 | 211.98 | 326.47 | 42.85 | Str. CC (61) |
| 95 | | | | 1590 | 124.45 | 234.28 | 30.61 | Str. CC (60) |
| 96 | | 1602vs | 1602vs | 1601 | 92.97 | 741.11 | 100.00 | Str. CC (48) |
| 97 | 1676vs | | | 1739 | 403.63 | 384.70 | 42.33 | Str. CC, OC (85) |
| 98 | | | | 2922 | 29.46 | 190.63 | 6.15 | Str. C–H (100) |
| 99 | 2970w | | | 2976 | 19.30 | 95.39 | 2.96 | Str. C–H (100) |
| 100 | | | | 3002 | 15.56 | 61.69 | 1.83 | Str. C–H (99) |

**Table 1.** (*Continued*)

| Mode no. | Experimental wavenumber ($cm^{-1}$) FT-IR | FT-Raman | Dispersive Raman | Scaled | Theoretical wavenumber ($cm^{-1}$) $IR_{int}$ | $S_{act}$ | $R_{Int}$ | TED (≥10%) |
|---|---|---|---|---|---|---|---|---|
| 101 | | | | 3054 | 5.67 | 75.00 | 2.12 | Str. C–H (98) |
| 102 | | | | 3058 | 3.30 | 34.18 | 0.96 | Str. C–H (99) |
| 103 | | | | 3065 | 11.25 | 145.09 | 4.05 | Str. C–H (99) |
| 104 | | 3068w | | 3069 | 31.84 | 60.23 | 1.67 | Str. C–H (99) |
| 105 | | | | 3071 | 5.02 | 149.33 | 4.15 | Str. C–H (99) |
| 106 | | | | 3079 | 33.81 | 132.52 | 3.67 | Str. C–H (99) |
| 107 | | | | 3086 | 16.11 | 1.11 | 0.03 | Str. C–H (97) |
| 108 | | | | 3087 | 5.26 | 6.22 | 0.17 | Str. C–H(99) |
| 109 | | | | 3088 | 0.56 | 80.08 | 2.18 | Str. C–H (97) |
| 110 | | | | 3089 | 9.06 | 113.56 | 3.10 | Str. C–H (93) |
| 111 | | | | 3089 | 3.72 | 251.70 | 6.87 | Str. C–H (98) |
| 112 | | | | 3100 | 6.69 | 52.04 | 1.40 | Str. C–H(97) |
| 113 | | | | 3103 | 2.36 | 149.58 | 4.03 | Str. C–H(96) |
| 114 | 3448w sh | | | 3555 | 89.16 | 215.59 | 3.69 | Str. O–H(100) |

$IR_{int}$, IR intensity (km $mol^{-1}$); $S_{act}$, Raman scattering activity ($Å^4$/amu); $R_{int}$, Raman intensity (arb units); w, weak; vw, very weak; mw, medium–weak; s, strong; vs, very strong; m, medium; br, sh, broad, shoulder; Str., stretching; Bend, bending; Tor., torsion. Energy values E(6-31G(d)) = −977.591085663 a.u.; E(6-311++G(d)) = −977.820319857 a.u.; E(6-311++G(d,p)) = −977.852629260 a.u.)

*COOH vibrations*

Carboxylic acid dimmer is formed by strong hydrogen bonding in the solid and liquid state. Vibrational analysis of the COOH group is made on the basis of the carbonyl and hydroxyl groups. The C═O stretching of carboxylic acids is identical to that in ketones, which is expected in the region 1740–1660 $cm^{-1}$.[39] The C═O bond formed by $P_\pi - P_\pi$ between the C and O intermolecular hydrogen bonding reduces the wavenumbers of the C═O stretching absorption to a greater degree than does the intermolecular H bonding because, due to the different electronegativities of C and O, the bondings are not equally distributed between the two atoms. The lone pair of electrons on the oxygen also determines the nature of the carbonyl groups. In the present study, a very strong band in the FT-IR spectrum at 1676 $cm^{-1}$ is assigned to the C═O stretching vibration and shows satisfactory agreement with the B3LYP/6-31G(d)-scaled value at 1739 $cm^{-1}$.

The free hydroxyl group absorbs strongly in the region 3700–3584 $cm^{-1}$, but the intermolecular-hydrogen bond formation can lower the O–H stretching wavenumber in the range 3500–3200 $cm^{-1}$ with increase in intensity and breadth.[40,41] The calculated wavenumber at 3555 $cm^{-1}$ shows a positive deviation of about ∼100 $cm^{-1}$ when compared with the literature value, which may be due to the presence of hydrogen bonding. The same behavior is in good agreement with the literature data.[42] The in-plane O–H deformation vibration usually appears as a strong band in the region 1440–1260 $cm^{-1}$ in the FT-IR spectrum.[43,44] The computed wavenumber for this mode is at 1339 $cm^{-1}$, which is assigned to the O–H in-plane bending vibrations. The O–H out-of-plane deformation vibration lies in the region 280–312 $cm^{-1}$ for free O–H and in the region 600–720 $cm^{-1}$ for associated O–HO–H.[17] In the present study, the O–H out-of-plane bending vibration appears as a weak band in the FT-IR spectrum at 638 $cm^{-1}$ and shows good agreement with the computed wavenumber at 618 $cm^{-1}$ by the B3LYP/6-31G(d) method. The potential energy distribution (TED) corresponding to this vibration is ∼45%.

*$CH_3$ vibration*

The molecule 4-[PBA] possesses one $CH_3$ group as shown in Fig. S2. For the $CH_3$ groups, one can expect nine fundamentals, which can be associated with each $CH_3$ group, namely the symmetrical stretching, the asymmetrical stretching, the symmetrical and asymmetrical deformation, the in-plane rocking, out-of-plane rocking and twisting bending.

The C–H stretching in $CH_3$ occurs at lower wavenumbers than those of aromatic rings (3000–3100 $cm^{-1}$). The asymmetric C–H stretching mode of the $CH_3$ group is expected in the region around 2980 $cm^{-1}$, and symmetric[44–47] one is expected around 2870 $cm^{-1}$. In the present study, the $CH_3$ asymmetric and symmetric stretching vibration computed by the B3LYP/6-31G(d) method is at 3002–2922 $cm^{-1}$ (mode nos. 100-98). The recorded spectrum shows only one band in this region at 2970 $cm^{-1}$ assignable to the $CH_3$ symmetric stretching vibration. The TED corresponding to this vibration is a pure mode contributing exactly 100%.

For methyl-substituted benzene derivatives, the asymmetric and symmetric deformation vibrations of the methyl group normally appear in the region 1465–1440 and 1390–1370 $cm^{-1}$, respectively.[47–49] Based on the literature data, in the present study the medium band observed in the FT-IR spectrum at 1423 $cm^{-1}$, in the FT-Raman at 1421 and 1420 $cm^{-1}$ and in the dispersive Raman as a weak band is assigned to $CH_3$ asymmetric deformation vibration. The theoretically computed value by the B3LYP/6-31G(d) method at 1421 $cm^{-1}$ (mode no. 84) shows good agreement with the literature values as well as experimental observations.

The theoretically predicted value by the B3LYP/6-31G(d) method at 1316 $cm^{-1}$ (mode no. 80) is assigned to $CH_3$ symmetric deformation vibrations of $CH_3$ group, which is also in good agreement with the above literature data as well as the measured FT-IR and FT-Raman value both at 1314 $cm^{-1}$. The dispersive Raman spectrum shows this band at 1312 $cm^{-1}$. The rocking vibrations of $CH_3$ modes usually appear[50] in the region

1070–1010 $cm^{-1}$. The band observed at 1028 $cm^{-1}$ in the FT-IR spectrum is assigned to the $CH_3$ rocking vibration. The theoretically computed value by the B3LYP/6-31G(d) method at 1032 $cm^{-1}$ (mode no. 61) is assigned to the $CH_3$ rocking vibration.

The $CH_3$ torsional vibrations are not observed in the FT-IR spectrum because these appear at very low wavenumbers. The theoretical wavenumber corresponding to this vibration is at 47 $cm^{-1}$ (mode no. 4). This means that the rotation of the methyl group is not significantly hindered. The C–$CH_3$ in-plane and out-of-plane bending vibrations computed by the B3LYP/6-31G(d) method also show good agreement with the experimental values as depicted in Table 1.

*C═N and C–N vibrations*

The identification of C–N and C═N vibrations is a very difficult task, as the mixing of several bands is possible in this region. Silverstein and Webster[41] assigned the C–N stretching absorption in the region of 1266–1382 $cm^{-1}$ for aromatic amines. In benzamide, the band observed at 1368 $cm^{-1}$ is assigned to C–N stretching.[50] In benzotriazole, the C–N stretching bands are found at 1307 and 1382 $cm^{-1}$. The theoretically computed wavenumber falls in the region 1301–1196 $cm^{-1}$ for the 4-[PBA] molecule. The bands at 1281 and 1280 $cm^{-1}$ in FT-IR and FT-Raman spectrum are assigned to C–N and C–C stretching vibrations, respectively. The same vibration in the dispersive Raman spectrum appears at 1279 $cm^{-1}$ as a very strong band and is assigned to the C–N stretching vibration. The TED corresponding to the vibrations is ~40% mixed with the C–C stretching vibration as shown in Table 1. The calculated IR intensity shows a maximum value, which matches well with the intensity in the IR spectrum.

*Ring vibrations*

Carbon–carbon ring stretching vibrations occur in the region of 1430–1625 $cm^{-1}$. In general, the bands due to this kind of bonding are of variable intensity and are observed at 1625–1590, 1575–1590, 1470–1540, 1430–1465 and 1280–1380 $cm^{-1}$ from the wavenumber ranges given by Varsanyi[43] for the five bands in the region. In the present work, the wavenumbers observed in FT-IR spectrum for 4-[PBA] in the range of 1676, 1584, 1509, 1488, 1423, 1281, 1175, 1129, 1082, and 1028 $cm^{-1}$ have been assigned to C–C stretching vibrations. The corresponding bands appear at 1602, 1502, 1421, 1280, 1177, 1155 and 1133 $cm^{-1}$ in the FT-Raman spectrum. In dispersive Raman, these bands are at 1602, 1502, 1420, 1177 and 1133 $cm^{-1}$. The theoretically computed wavenumbers for this vibration lie in the range of 1739–1478, 1441–1406, 1339 and 1311–1016 $cm^{-1}$ (mode nos. 97-88, 85-83, 81, 79-60) by the B3LYP/6-31G(d) method, and show excellent agreement with the experimental spectral data.

Shimanouchi *et al.*[51] reported the wavenumber data of these vibrations in different benzene derivatives through normal coordinate analysis. The bands observed at 451 and 421 $cm^{-1}$ in the FT-IR spectrum are assigned to C–C–C deformation of the phenyl ring. The C–C–C in-plane and out-of-plane bending vibrations computed by the B3LYP/6-31G(d) method show good agreement with the experimental observations, as depicted in Table 1.

## NBO analysis

NBO analysis provides the most accurate possible 'natural Lewis structure' picture of $\phi$, because all orbital details are mathematically chosen to include the highest possible percentage of the electron density (ED). A useful aspect of the NBO method is that it gives information about interactions in both filled and virtual orbital spaces that could enhance the analysis of intra- and intermolecular interactions.

The second-order Fock matrix evaluation was carried out to elucidate the donor–acceptor interactions in the NBO analysis.[52] The result of these interactions is a loss of occupancy from the localized NBO of the idealized Lewis structure into an empty non-Lewis orbital. For each donor ($i$) and acceptor ($j$), the stabilization energy ($E_2$) associated with the delocalization $i \rightarrow j$ is estimated as

$$E_2 = \Delta E_{ij} = q_i \frac{F(i,j)^2}{\varepsilon_j - \varepsilon_i}$$
$$E_2 = \Delta E_{ij} = q_i \frac{F(i,j)^2}{\varepsilon_j - \varepsilon_i} \quad (2)$$

where $q_i$ is the donor orbital occupancy, $\varepsilon_i$ and $\varepsilon_j$ are diagonal elements and $F(i,j)$ is the off-diagonal element of the NBO Fock matrix.

NBO analysis provides an efficient method for studying the intra- and intermolecular bonding and interaction among bonds, and is also a convenient basis for investigating charge transfer or conjugative interaction in molecular systems. Some electron donor orbital, acceptor orbital and the interacting stabilization energy resulting from the second-order micro-disturbance theory have been reported.[53,54] The larger the $E_2$ value, the more intense is the interaction between electron donors and electron acceptors (i.e. the more the donating tendency from electron donors to electron acceptors, the greater the extent of conjugation of the whole system). Delocalization of ED between occupied Lewis-type (bonding or lone pair) NBO orbitals and formally unoccupied (antibonding or Rydgberg) non-Lewis NBO orbitals corresponds to a stabilizing donor–acceptor interaction. NBO analysis has been performed on the molecule at the DFT/B3LYP/6-31G(d) level in order to elucidate the intramolecular interactions, rehybridization and delocalization of ED within the molecule.

The intramolecular interactions are due to the orbital overlap between bonding C–C, C–N and C═O antibonding orbitals, which results in an intramolecular charge transfer (ICT) causing stabilization of the system. These interactions are observed when there is an increase in ED in C–C, C–N and C═O antibonding orbitals, which weakens the respective bonds. The ED of two conjugated single as well as double bonds of three aromatic rings lies between 1.6 and 1.97e, clearly demonstrating strong delocalization for the 4-[PBA] molecule. The strong intramolecular hyperconjugative interaction of the $\sigma$ and $\pi$ electrons of the C–C bond with the anti C–C bond of the ring leads to stabilization of some part of the ring, as evidenced from Table S2. For example, the intramolecular hyperconjugative interaction of the $\sigma$ bond (C14–C17) distributes to $\sigma^*$ (N1–C12, C12–C14), leading to stabilization of 4 kJ/mol. This interaction enhanced the conjugation further with the antibonding orbital of $\pi^*$(C12–C13, C15–C19), which leads to a strong delocalization of 20 kJ/mol. The same kind of interaction is calculated for C15–C19, C22–C23, C24–C27 and C25–C29 bonds, as shown in Table S2. The interaction energy, which is related to the resonance in the molecule, is electron withdrawing to the ring from the loan through $\sigma^*$ as well as $\pi^*$ to the ring as shown in Table S2. The $\pi^*$ C12–C13 bond conjugated to the $\pi^*$ C14–C17 shows

an enormous amount of stabilization energy (240.21 kJ/mol), as depicted in Table S2.

## Conclusion

The experimental and theoretical spectra obtained from Raman (dispersive and FT-Raman) and FT-IR measurements of the 4-[PBA] molecule are reported for the first time. Theoretical simulations predict the equilibrium geometry of the molecule to belong to the lowest ($C_1$) symmetry. Good agreement between experimental and theoretically calculated spectra allowed positive assignment of all the observed FT-IR and FT-Raman and dispersive Raman bands, which indicates that the theoretically optimized geometry of the 4-[PBA] molecule closely matches with the crystal data of the related triphenylamine molecule. NBO analysis confirms the intramolecular charge transfer occurring mainly from the methyl group.

### Acknowledgements

This work was supported by TUBITAK under Grant No. TBAG-108T718, Turkey.

### Supporting information

Supporting information may be found in the online version of this article.

## References

[1] W. L. Yu, J. Pei, W. Huang, A. J. Heeger, *Chem. Commun.* **2000**, 681.
[2] J. P. Chen, H. Tanabe, X. C. Li, T. Thoms, Y. Okamura, K. Veno, *Synth. Met.* **2003**, *132*, 173.
[3] F. L. Bai, M. Zheng, G. Yu, D. B. Zhu, *Thin Solid Films* **2000**, *363*, 118.
[4] D. Troades, G. Veriot, A. Moliton, *Synth. Met.* **2002**, *127*, 165.
[5] T. Noda, Y. Shirota, *J. Lumin.* **2000**, *87*, 1168.
[6] C. S. Ha, J. H. Shin, H. Lim, W. J. Cho, *Mater. Sci. Eng.* **2001**, *13*((85)), 195.
[7] R. A. Holroyd, J. M. Preses, E. H. Boettcher, W. F. Schmid, *J. Phys. Chem.* **1984**, *88*, 744.
[8] J. Ostrauskaite, H. R. Karickal, L. Leopold, D. Haarer, M. Thelakkat, *J. Mater. Chem.* **2002**, *12*, 58.
[9] Y. Yasuda, T. Kamiyama, Y. Shirota, *Electrochim. Acta* **2000**, *45*, 1537.
[10] J. Steiger, R. Schmechel, H. Von Seggern, *Synth. Met.* **2009**, *129*, 1.
[11] C. W. Tang, S. A. Van Slyke, *Appl. Phys. Lett.* **1987**, *51*, 913.
[12] C. W. Tang, S. A. Van Slyke, C. H. Chen, *J. Appl. Phys.* **1989**, *65*, 3610.
[13] M. X. Yu, J. P. Duan, C. H. Lin, C. H. Cheng, Y. T. Tao, *Chem. Mater.* **2002**, *14*, 3958.
[14] I. Y. Wu, J. T. Lin, Y. T. Tao, E. Balasubramaniam, Y. Z. Su, C. W. Ko, *Chem. Mater.* **2001**, *13*, 2626.
[15] J. Salkbeck, N. Yu, F. Weissotel, J. Bauer, H. Bestgen, *Synth. Met.* **1997**, *91*, 209.
[16] H. H. Fong, K. C. Lun, S. K. So, *Chem. Phys. Lett.* **2002**, *353*, 407.
[17] Y. Shirota, K. Okumoto, H. Inada, *Synth. Met.* **2000**, *111*, 387.
[18] P. M. Borsenberger, E. H. Magin, *J. Shi. Phys. B* **1996**, *217*, 212.
[19] E. W. Forsythe, M. A. Abkowitz, Y. Gao, *J. Phys. Chem. B* **2000**, *104*, 3948.
[20] K. Naito, A. Miura, *J. Phys. Chem.* **1993**, *97*, 6240.
[21] E. Lebedev, T. Dittrich, V. Petrova-Koch, S. Karg, W. Brutting, *Appl. Phys. Lett.* **1997**, *71*, 2686.
[22] N. Pan, J. Elliott, H. Hendriks, L. Aucoin, P. Fay, I. Adesida, *Appl. Phys. Lett.* **1995**, *66*(2), 212.
[23] S. Sebastian, N. Sundaraganesan, S. Manoharan, *Spectrochim. Acta* **2009**, *A74*, 312.
[24] J. P. Abraham, I. H. Joe, V. George, O. F. Nielson, V. S. Jayakumar, *Spectrochim. Acta* **2003**, *59A*, 193.
[25] J. Binoy, J. P. Abraham, I. H. Joe, V. S. Jayakumar, J. Aubard, O. F. Nielson, *J. Raman Spectrosc.* **2005**, *36*, 63.
[26] M. C. Harris, S. L. Buchwald, *J. Org. Chem.* **2000**, *65*, 5327.
[27] J. Dash, P. S. Shirude, S.-T. Danny Hsu, S. Balasubramanian, *J. Am. Chem. Soc.* **2008**, *130*, 15950.
[28] Gaussian Inc. *Gaussian 09 Program*, Gaussian Inc.: Wallingford, CT, **2009**.
[29] H. B. Schlegel, *J. Comput. Chem.* **1982**, *3*, 214.
[30] G. Keresztury, S. Holly, J. Varga, G. Besenyei, A. Y. Wang, J. R. Durig, *Spectrochim. Acta* **1993**, *49A*, 2007.
[31] G. Keresztury, J. M. Chalmers, P. R. Griffith (Eds), *Raman Spectroscopy: Theory, Hand book of Vibrational Spectroscopy*, vol. 1, John Wiley & Sons Ltd.: New York, **2002**.
[32] J. Baker, A. A. Jarzccki, P. Pulay, *J. Phys. Chem.* **1998**, *102A*, 1412.
[33] P. Pulay, J. Baker, K. Wolinski, SQM, 2013 Green Arc Road, Suite A, Fayettevile, AR72703, USA.
[34] E. D. Glendening, A. E. Reed, J. E. Carpenter, F. Weinhold, NBO Version 3.1, TCI, University of Wisconsin, Madison, **1998**.
[35] A. N. Sobolev, V. K. Belsky, I. P. Romm, N. Yu. Chernikova, E. N. Gurianova, *Acta. Crystallogr.* **1985**, *C41*, 967.
[36] I. Reva, L. Lapinski, N. Chattopadhyay, R. Fausto, *Phys. Chem. Chem. Phys.* **2003**, *5*, 3844.
[37] A. P. Scott, L. Radom, *J. Phys. Chem.* **1996**, *100*, 16502.
[38] G. Varsanyi, *Assignments of Vibrational Spectra of Seven Hundred Benzene Derivatives*, vol. 1–2 Adam Hilger, **1974**.
[39] D. L. Vein, N. B. Colthup, W. G. Fateley, J. G. Grasselli, *The Handbook of Infrared and Raman Characteristic Frequencies of Organic Molecules*, Academic Press: San Diego, **1991**.
[40] B. Smith, *Infrared Spectral Interpretation, A Systematic Approach*, CRC Press: Washington, DC, **1999**.
[41] R. M. Silverstein, F. X. Webster, *Spectroscopic Identification of Organic Compounds* (6th edn), John Wiley & Sons Inc.: New York, **2003**.
[42] V. Krishnakumar, R. Mathammal, S. Muthunatesan, *Spectrochim. Acta* **2008**, *70A*, 201.
[43] G. Varsanyi, *Vibrational Spectra of Benzene Derivatives*, Academic Press: New York, **1969**.
[44] G. Socrates, *Infrared Characteristic Group Frequencies*, John Wiley and Sons: New York, **1980**.
[45] D. A. Kleinman, *Phys. Rev.* **1962**, *126*, 1977.
[46] N. B. Colthup, L. H. Daly, S. E. Wiberly, *Introduction to Infrared and Raman Spectroscopy*, Academic Press: New York, **1990**.
[47] B. Venkataram Reddy, G. Ramana Rao, *Vib. Spectrosc.* **1994**, *6*, 231.
[48] J. F. Areanas, I. Lopez Tacon, J. C. Otero, J. I. Marcos, *J. Mol. Struct.* **1997**, *267*, 410.
[49] D. A. Long, W. O. Jeorge, *Spectrochim. Acta* **1963**, *19*, 1777.
[50] R. Shanmugam, D. Sathyanarayana, *Spectrochim. Acta* **1984**, *40A*, 764.
[51] T. Shimanouchi, Y. Kakiuti, I. Gamo, *J. Chem. Phys.* **1956**, *25*, 1245.
[52] M. Szafran, A. Komasa, E. B. Adamska, *J. Mol. Struct. (THEOCHEM)* **1956**, *827*, 101.
[53] C. James, A. Amal Raj, R. Reghunathan, I. Hubert Joe, V. S. Jayakumar, *J. Raman Spectrosc. 37*, **2006**, 1381.
[54] L. Jun-na, C. Zhi-Rang, Y. Shen-Fang, *J. Zhejiang Univ. Sci. 6B*, **2005**, 584.